INSTITUTE FOR FUSION STUDIES

DOE/ET-53088-451 IFSR #451

Effects of Compressibility, Diamagnetic Drift, and Thermal Conduction on Resistive Ballooning Modes in the Second Stability Regime

JIN-YONG KIM, D.-I. CHOI,[1] J.W. VAN DAM, and W. HORTON
Institute for Fusion Studies
The University of Texas at Austin
Austin, Texas 78712

[1] *Korea Advanced Institute of Science & Technology, P.O. Box 150, Cheongyangni, Seoul, Korea*

August 1990

THE UNIVERSITY OF TEXAS

AUSTIN

Effects of Compressibility, Diamagnetic Drift, and Thermal Conduction on Resistive Ballooning Modes in the Second Stability Regime

Jin-Yong Kim, D.-I. Choi,[a] J.W. Van Dam, and W. Horton
Institute for Fusion Studies
The University of Texas at Austin
Austin, Texas 78712

Abstract

The stabilizing effects of various terms such as compressibility, diamagnetic drift, and parallel thermal conduction are investigated on the type of resistive ballooning modes whose driving force comes from the resistive region, which are known to be unstable in the high-beta second stability regime when analyzed in the incompressible limit. We find that compressibility gives a significant stabilizing effect mainly through the perpendicular magnetic compression, which suggests the possibility of a second stable window for these resistive ballooning modes. The diamagnetic drift terms slightly reduce the growth rate in the incompressible limit, but, with finite compressibility, lead to fairly strong stabilization. The compression due to ion polarization, which becomes significant at large diamagnetic drift, contributes to this stabilization. On the other hand, parallel thermal conduction and perpendicular magnetic compression, which enter through the equation for temperature evolution, are shown to have a negligible effect on the stability of these modes.

[a]Permanent address: Korea Advanced Institute of Science & Technology, P.O. Box 150, Cheongyangni, Seoul, Korea

I. Introduction

Recently, there has been considerable interest in the second stability regime, where the ideal ballooning modes are re-stabilized. A number of studies have been carried out in order to determine the ideal marginal stability boundary under various conditions and to find various methods for reducing the size of the gap between the first and second stability regime. However, tokamak plasmas that are stable against ideal ballooning modes can still be unstable with respect to resistive ballooning modes. Therefore the investigation of their stability is an important related problem.

Recently, Sykes *et al.*[1] showed numerically that in most of the second stability regime, the well-known parameter Δ', which represents the driving force coming from the ideal region of the resistive ballooning mode, is negative. This result, which was analytically confirmed by Fu *et al.*,[2] suggests that the resistive ballooning modes driven by Δ' will be stabilized. However, as has shown in previous papers,[3,4] there also exists another branch of resistive ballooning modes, which can be unstable in the second stability regime due to a different non-Δ' type of driving force coming from the resistive region. Recently, Hender *et al.*[5] have carried out a numerical study of these unstable modes in the compressible model and found that these modes are significantly stabilized when the plasma pressure is increased. Their results indicate the possibility of a second stable window for these resistive ballooning modes.

The present work is a generalization of our previous paper,[4] which employed the incompressible model, to a more advanced model that includes finite compressibility and also the effects of diamagnetic drift and parallel thermal conduction. Since these terms are proportional to the plasma pressure, they can become significant in the high-beta second stability regime. This feature motivated our investigation of their effects. Here, as in our earlier study, we employ the well-known s-α equilibrium model for tokamaks, for simplicity.

First, the effect of finite compressibility will be considered in detail. We find that com-

pressibility contributes to significant stabilization, in agreement with the results of Hender *et al.*[5] The main stabilizing effect comes from the perpendicular magnetic compression. This conclusion is similar to that found in an earlier study by Hender *et al.*[6] of the low-beta first stability regime. However, this feature of the effect of compressibility on the present modes differs greatly with the case of the resistive ballooning modes driven by Δ', on which the perpendicular magnetic compression has a negligible effect.

The effect of the diamagnetic drift has been previously investigated by Diamond *et al.*[7] in the incompressible limit and in the first stability regime. They found that the effect of non-zero diamagnetic drift is to reduce the growth rate slightly. Here, we study the diamagnetic drift effect in the two cases of an incompressible plasma and a compressible plasma for the second regime of stability. We find that the effect is similar to that found by Diamond *et al.*[7] in the incompressible limit, but with finite compressibility, the diamagnetic drift leads to a fairly large stabilizing effect. The compression due to ion polarization, which becomes significant at large values of the diamagnetic drift, is shown to give a stabilizing effect, contrary to its effect on the modes driven by Δ'.[8]

For the effect of parallel thermal conduction, Sundaram *et al.*[9] performed an approximate analytical study in the first stability regime and concluded that for moderately large β values all resistive ballooning modes may be stabilized completely by this effect. Our study shows that the parallel thermal conduction has a negligible effect on the present modes in the second stability regime. This feature is also different from the case of the modes that are driven by Δ'.[10]

The outline of this paper is as follows. In Sec. II, our model equations are presented. Numerical results and discussion for various limiting cases are given in Sec. III. Finally, our conclusions are summarized in Sec. IV.

II. Basic Equations

We start from the linearized resistive MHD equations derived by Connor *et al.*[11] The equations were obtained from the full set of the Braginskii two-fluid equations with the use of the ballooning mode representation. They include the diamagnetic drift, compression, viscosity, and thermal conduction and transport terms. Here we limit our interest to the cold ion model in which full electron dynamics are retained and ion viscosity terms are neglected. Then, since we will also neglect small terms of order β, the equations become

$$\frac{\mathbf{B}\cdot\boldsymbol{\nabla}}{B}\left(\frac{e\phi}{T}-1.71\frac{t}{T}-\frac{n}{N}\right)=-\frac{ea_{\|}}{cT}\left[\gamma+i\omega_{*}(1+1.71\eta_{e})+\frac{\eta_{\|}c^{2}k_{\perp}^{2}}{4\pi}\right], \tag{1}$$

$$\mathbf{B}\cdot\boldsymbol{\nabla}\left(\frac{ck_{\perp}^{2}a_{\|}}{4\pi NeB}\right)=-\gamma b_{s}\frac{e\phi}{T}-2i\omega_{\rho}\frac{p}{P}, \tag{2}$$

$$\frac{\mathbf{B}\cdot\boldsymbol{\nabla}}{\gamma\rho B}\left[\frac{\mathbf{B}\cdot\boldsymbol{\nabla}p}{B}+i\omega_{*}(1+\eta_{e})\frac{Nea_{\|}}{c}\right]=\gamma\frac{n}{N}+\frac{e\phi}{T}(\gamma b_{s}+i\omega_{*}+2i\omega_{\rho})-\frac{\eta_{\perp}k_{\perp}^{2}c^{2}p}{B^{2}}, \tag{3}$$

$$\begin{aligned}\frac{K_{\|e}}{N}\mathbf{B}\cdot\boldsymbol{\nabla}\left[\frac{\mathbf{B}\cdot\boldsymbol{\nabla}}{B^{2}}\left(\frac{t}{T}\right)-i\frac{a_{\|}e}{cT}\frac{\omega_{*}\eta_{e}}{B}\right]+\frac{0.71}{Ne}\mathbf{B}\cdot\boldsymbol{\nabla}\left(\frac{k_{\perp}^{2}a_{\|}c}{4\pi B}\right)-\frac{K_{\perp e}k_{\perp}^{2}}{N}\frac{t}{T}\\ =\frac{3}{2}\gamma\frac{t}{T}-5i\omega_{\rho}\frac{t}{T}-\gamma\frac{n}{N}-i\omega_{*}\left(1-\frac{3}{2}\eta_{e}\right)\frac{e\phi}{T},\end{aligned} \tag{4}$$

where γ is the growth rate; $\omega_{*}=\boldsymbol{\nabla}N\times\mathbf{B}\cdot\mathbf{k}_{\perp}\frac{cT_{e}}{NeB^{2}}$ is the diamagnetic drift frequency due to the density gradient; $\eta_{e}=\frac{d\ln T_{e}}{d\ln N}$; $\eta_{\|}=\frac{m_{e}\nu_{e}}{Ne^{2}}$ is the parallel resistivity; $\eta_{\perp}=1.96\eta_{\|}$; $\mathbf{k}_{\perp}$ is the perpendicular wavenumber vector; $b_{s}=k_{\perp}^{2}\rho_{s}^{2}$, with $\rho_{s}^{2}=\frac{T_{e}}{m_{i}\omega_{ci}^{2}}$ and $\omega_{ci}=\frac{eB}{m_{i}c}$; $\rho=m_{i}N$; $K_{\|e}=\frac{3.2P_{e}}{m_{e}\nu_{e}}$; $K_{\perp e}=\frac{4.7P_{e}\nu_{e}}{m_{e}\omega_{ce}^{2}}$; $\nu_{e}=\frac{4\sqrt{2\pi}N\lambda e^{4}}{\sqrt{m_{e}}T_{e}^{3/2}}$; $\omega_{\rho}=\boldsymbol{\kappa}\times\mathbf{b}\cdot\mathbf{k}_{\perp}\frac{cT_{e}}{eB}$ is the magnetic curvature drift frequency, with $\boldsymbol{\kappa}=(\mathbf{b}\cdot\boldsymbol{\nabla})\mathbf{b}$ and $\mathbf{b}=\frac{\mathbf{B}}{B}$. The dependent variables n, ϕ, p, $a_{\|}$, and t represent the density, electrostatic potential, pressure, vector potential, and temperature perturbations, respectively. Also, Eqs. (1)–(4) represent, respectively, the parallel Ohm's law, the quasineutrality condition, the continuity equation, and the equation

for temperature evolution. The physical meaning of each term in the equations will be described later in this section.

Now, we apply the $s-\alpha$ tokamak equilibrium model for the limit of large aspect ratio and circular flux surfaces. Then, to the lowest order in the inverse aspect ratio, we have

$$\frac{\mathbf{B}\cdot\boldsymbol{\nabla}}{B} = \frac{1}{Rq}\frac{\partial}{\partial\theta} ,$$

$$k_\perp^2 = \frac{n^2q^2}{r^2}f(\theta) ,$$

$$\omega_* = -\frac{cnqT_e}{rNeB}\frac{dN}{dr} ,$$

$$\omega_\rho = -\frac{cnqT_e}{reB}\left[\cos\theta + \sin\theta\ I(\theta)\right] ,$$

where

$$f(\theta) = 1 + I^2(\theta) ,$$

$$I(\theta) = s(\theta-\theta_o) - \alpha\sin\theta ,$$

$$\alpha = -\frac{2Rq^2}{B^2}\frac{dp}{dr} .$$

With these representations for the various equilibrium quantities, after some normalization we can obtain the following forms for Eqs. (1)–(4) :

$$\frac{\partial}{\partial\theta}\left(\phi + \frac{i\widehat{\omega}_*}{\widehat{\gamma}}p + \alpha_1\frac{i\widehat{\omega}_*}{\widehat{\gamma}}t\right) = \left[1 + \frac{i\widehat{\omega}_*}{\widehat{\gamma}}(1+\alpha_2\eta_e) + \frac{\epsilon}{\widehat{\gamma}}f\right]\psi , \tag{5}$$

$$\frac{\partial}{\partial\theta}(f\psi) = \epsilon\widehat{\gamma}^2 f\phi - \frac{C}{1+\eta_e}p , \tag{6}$$

$$\frac{\partial}{\partial\theta}\left(\frac{\partial p}{\partial\theta} - \psi\right) = G\widehat{\gamma}^2(p-\phi-t) + 2\epsilon_n G\widehat{\gamma}^2\frac{C}{\alpha}\phi + M_\perp\widehat{\gamma}\epsilon^2 fp + i\widehat{\omega}_*\widehat{\gamma}^3 Kf\phi , \tag{7}$$

$$\alpha_3\nu\frac{\partial}{\partial\theta}\left[\frac{\partial t}{\partial\theta} - \left(\eta_e + \frac{i\alpha_1\epsilon}{\omega_*\alpha_3}f\right)\psi\right] = \alpha_4\epsilon^2 ft + G\widehat{\gamma}\left[\frac{5}{2}t - p + \left(1-\frac{3}{2}\eta_e\right)\phi\right] + 5i\widehat{\omega}_*\epsilon_n G\frac{C}{\alpha}t , \tag{8}$$

where

$$\psi = -\frac{\gamma e R q}{c T_e} a_{||}, \quad \phi_{\rm new} = \frac{e\phi_{\rm old}}{T_e}, p_{\rm new} = \frac{i\gamma p_{\rm old}}{\omega_* P_e}, \quad t_{\rm new} = \frac{i\gamma t_{\rm old}}{\omega_* T_e} ,$$

$$\widehat{\gamma} = \frac{\gamma}{\gamma_r}, \quad \widehat{\omega}_* = \frac{\omega_*}{\gamma_r}, \quad \gamma_r = \left(\frac{n^2 q^2}{\tau_r \tau_A^2}\right)^{\frac{1}{3}}, \quad \epsilon = \left(\frac{n^2 q^2}{S_R}\right)^{\frac{2}{3}} ,$$

$$S_R = \frac{\tau_r}{\tau_A}, \quad \tau_r = \frac{4\pi r^2}{\eta_{||} c^2}, \quad \tau_A = \frac{Rq}{\sqrt{B^2/4\pi\rho}} ,$$

$$G = \frac{\epsilon}{\beta}, \quad M_\perp = \frac{\eta_\perp}{\eta_{||}}, \quad K = K_o G^2, \quad K_o = \frac{\epsilon_n^2}{q^2} = \frac{2\epsilon_n \beta}{\alpha} ,$$

$$\beta = \frac{4\pi P_e}{B^2}, \quad \nu = \frac{m_i \gamma_r}{m_e \nu_e}, \quad \epsilon_n = -(\frac{RdN}{Ndr})^{-1} ,$$

$$\alpha_1 = 0.71, \quad \alpha_2 = 1 + \alpha_1, \quad \alpha_3 = 3.2, \quad \alpha_4 = 4.7 ,$$

$$C = \alpha \left[\cos\theta + \sin\theta \; I(\theta)\right] .$$

Now we explain the physical meaning of each term in the equations. In the parallel Ohm's law, Eq. (5), the first terms on the left-hand side and on the right-hand side are the electrostatic and the electromagnetic parts of the parallel electric field; the terms with ω_* are due to the parallel electron pressure gradient; and the terms with α_1 come from the parallel thermal force. In the vorticity equation, Eq. (6), the term on the left-hand side describes the field line bending; the first term on the right-hand side is the inertia; and the second term on the right-hand side represents the ballooning driving force. In the continuity equation, Eq. (7), the term on the left-hand side is the parallel ion sound compression term; the first term on the right-hand side is the density convection; the term with ϵ_n comes from the compression of the $\mathbf{E} \times \mathbf{B}$ drift and is called the perpendicular magnetic compression term; the term with $M_\perp$ is the perpendicular transport; and the last term is the ion polarization. In the temperature evolution equation, Eq. (8), the terms on the left-hand side describe parallel thermal conduction; the first term on the right-hand side is the

perpendicular thermal transport; the second set of terms, all multiplied by the coefficient G, come from the convection of the temperature; and the last term arises from the compression of the $\mathbf{E} \times \mathbf{B}$ drift.

III. Numerical Results and Discussion

For simplicity, we will separately study the effects of compression, diamagnetic drift, and parallel thermal conduction. With some assumptions, we are able to reduce the basic equations, Eqs. (5)–(8), to a fourth-order differential equation in each case. We solve these equations using two different numerical codes. One is a standard eigenvalue package,[12] and the other is a shooting code that we have developed. We checked the reliability of each code by testing whether the results are sensitive to the size of the mesh interval as an accuracy parameter. We find that the results from the two methods are in good agreement within the parameter range where both methods are valid. The numerical results are also compared with some approximate analytic results which are obtained by means of a flux-surface averaging procedure based on a two scale length assumption. In Sec. III.A we present a detailed numerical analysis of the compression effect. We next treat the diamagnetic drift effect in Sec. III.B and, finally, the parallel thermal conduction effect in Sec. III.C.

A. Effect of Compression

In this section, we omit the diamagnetic drift terms and temperature gradient terms. We also neglect the temperature evolution equation, Eq. (8), and investigate in detail only the effect of compression. The basic set of Eqs. (5)–(8) then reduces to the following equations:

$$\frac{\partial}{\partial\theta}\phi = \left(1 + \frac{\epsilon}{\widehat{\gamma}} f\right)\psi \,, \tag{9}$$

$$\frac{\partial}{\partial\theta}(f\psi) = \epsilon\widehat{\gamma}^2 f\phi - Cp \,, \tag{10}$$

$$\frac{\partial}{\partial\theta}\left(\frac{\partial p}{\partial\theta}-\psi\right)=G\hat{\gamma}^2(p-\phi)+2\epsilon_n G\hat{\gamma}^2\frac{C}{\alpha}\phi+M_\perp\hat{\gamma}\epsilon^2 fp\ . \tag{11}$$

First, we present the numerical solution of these equations in Fig. 1, where the growth rate is given as a function of α in the second stability regime with $S=1$, $\epsilon=0.1$, $\beta=0.1$, and $\epsilon_n=0.1$. For comparison, we also show the numerical results in the incompressible case, which was studied in our previous paper.[4] It is seen that the compression gives a significant stabilizing effect.

In Fig. 1, we also present the solution that is obtained from the approximate dispersion relation

$$\hat{\gamma}^3+\frac{\hat{\gamma}}{G}(1+2q^2)=\frac{\alpha^2}{2}\ . \tag{12}$$

This dispersion relation can be straightforwardly derived from Eqs. (9)–(11) by flux-surface averaging under the assumption of two length scales with the orderings $\epsilon/\hat{\gamma}\ll 1$ and $G\hat{\gamma}^2\sim 1$. In Eq. (12), the compression effects are represented by the two terms in the parenthesis, where the first of these two terms comes from the parallel ion sound compression and the second comes from the perpendicular magnetic compression (i.e, the compression of the $\mathbf{E}\times\mathbf{B}$ drift). The large difference of the analytic solution with the exact numerical result seems to be caused by the failure of the two length scale assumption that was used to derive the analytic dispersion relation in the parameter regime with $\epsilon=0.1$ (the assumption applies well when $\epsilon\ll 1$).

However, this analytic result does suggest that significant stabilization may come from the perpendicular magnetic compression, since $q\geq 1$ in tokamaks. To clarify this question, we numerically investigated the explicit effect of each compression term. Our results are shown in Fig. 2, where the growth rate is given as a function of the parameter ϵ_n, which represents the magnitude of the perpendicular magnetic compression. The $\beta=0$ (or $G=\infty$) case in Fig. 2 corresponds to the case when, of the various compression terms, only the perpendicular magnetic compression term exists, as can be seen from Eq. (11). The difference between the

$\beta = 0$ and $\beta = 0.1$ cases is due to effects arising from the other types of compression, namely, the parallel ion sound compression and the perpendicular transport compression. Figure 2 shows that as ϵ_n increases, the dominant stabilization effect comes from the perpendicular magnetic compression among the various compression terms. In the regime where the mode is almost completely stabilized, the solution changes from a purely growing mode to a mode with a real frequency. We find that the mode is almost completely stabilized for $\epsilon \geq 0.15$, which is within the parameter regime of most tokamaks and also within the regime of validity of our large aspect ratio $s - \alpha$ equilibrium model. If we note that the modes with $\epsilon = 0.1$ investigated in Fig. 2 correspond to those with toroidal mode number $n \geq 100$ at values of $S_R \geq 10^6$ and $q = 2$ for the magnetic Reynolds number and safety factor, respectively, then this result suggests that most resistive ballooning modes within a moderate toroidal mode number range (≤ 100) may be stabilized in some part of the second stability regime, so that it may be possible for a second stable window for the resistive ballooning modes to exist, as was reported by Hender *et al.*[5]

B. Effect of Diamagnetic Drift

As mentioned earlier in Introduction, the diamagnetic drift and the parallel thermal conduction can become significant in the second stability regime where the β value is finite. Here, we study the effect of the diamagnetic drift in the incompressible limit and also in the compressible limit. The necessary equations are obtained from the Eqs. (5)–(8) as follows:

$$\frac{\partial}{\partial\theta}\left(\phi + \frac{i\hat{\omega}_*}{\hat{\gamma}}p\right) = \left(1 + \frac{i\hat{\omega}_*}{\hat{\gamma}} + \frac{\epsilon}{\hat{\gamma}}f\right)\psi \,, \tag{13}$$

$$\frac{\partial}{\partial\theta}(f\psi) = \epsilon\hat{\gamma}^2 f\phi - Cp \,, \tag{14}$$

$$\frac{\partial}{\partial\theta}\left(\frac{\partial p}{\partial\theta} - \psi\right) = G\hat{\gamma}^2(p-\phi) + 2\epsilon_n G\hat{\gamma}^2\frac{C}{\alpha}\phi + M_\perp\hat{\gamma}\epsilon^2 fp + i\hat{\omega}_*\hat{\gamma}^3 Kf\phi \,. \tag{15}$$

First, we consider the incompressible limit in which Eq. (15) reduces to $p = \phi$. Figure 3

shows the growth rate and real frequency as a function of the diamagnetic drift frequency $\widehat{\omega}_*$ for an incompressible plasma in the second stability regime with $\alpha = 4$, $s = 1$, and $\epsilon = 0.1$. The growth rate is slightly reduced as $\widehat{\omega}_*$ increases, similar to the result of Diamond *et al.*[7] in the first stability regime. The real frequency is much smaller than the diamagnetic frequency. Also shown in Fig. 3 are the growth rate and real frequency given by the analytical dispersion relation for the incompressible case,

$$\widehat{\gamma}^3 + i\widehat{\omega}_*\widehat{\gamma}^2 = \frac{1}{2}\alpha^2 \ . \tag{16}$$

As before, this is derived by the two-length-scale averaging procedure. It has the approximate solutions

$$\widehat{\gamma} \cong \begin{cases} \left(\dfrac{\alpha^2}{2}\right)^{1/3} - i\left(\dfrac{\widehat{\omega}_*}{3}\right) & \text{for } \widehat{\omega}_* \ll \widehat{\gamma} \\ \left(\dfrac{\alpha^2}{2\widehat{\omega}_*}\right)^{1/2}\left(\dfrac{1-i}{\sqrt{2}}\right) & \text{for } \widehat{\omega}_* \gg \widehat{\gamma} \ . \end{cases} \tag{17}$$

The analytical results (dashed curves) in Fig. 3 are in agreement with the numerical results (solid curves).

Next, we consider the compressible limit. The numerical results with compressibility included are given in Fig. 4, with $\alpha = 4$, $s = 1$, $\epsilon = 0.1$, and $\epsilon_n = 0.1$. Figure 4 clearly shows that the effect of the diamagnetic drift is strongly stabilizing for non-zero compressibility. The real frequency first increases and then decreases as $\widehat{\omega}_*$ increases. Figure 4 also shows the growth rate and the real frequency (dashed curves) given by the analytic dispersion relation

$$\widehat{\gamma}\left[1 + G\widehat{\gamma}^2\left(1 + \frac{i\widehat{\omega}_*}{\widehat{\gamma}}\right)\right] = \frac{\alpha^2}{2}G\left(1 - \frac{2\widehat{\gamma}\epsilon_n}{\alpha\epsilon}\right) \tag{18}$$

corresponding to the compressible limit.

We also note that the compression term that is closely associated with the finite diamagnetic drift is the ion polarization compression term, which is the last term in Eq. (15). Hence, we investigated the effect of this term, which can be conveniently performed by artificially

varying the proportionality factor K_o in the coefficient of the term. The results are given in Fig. 5 for $\widehat{\omega}_* = 1$. We find that the ion polarization compression contributes to a significant stabilization of the resistive ballooning modes. We note that this result is in contrast with the behavior for the case of the resistive ballooning modes driven by Δ', for which its effect is destabilizing.[8]

For the typical parameters of $\nu_e \sim 10^5$, $\rho_s/r \sim 10^{-2}$, $c_s/r_n \sim 10^5$, $q \sim 2$, and $\alpha = 2\beta q^2/\varepsilon_n \sim 4$, we estimate that the normalized diamagnetic drift frequency $\widehat{\omega}_* = \omega_*/\gamma_r$ can be much larger than unity for toroidal mode numbers in the range $n \geqq 10$. The results shown in Figs. 4 and 5 then suggest that due to this large diamagnetic drift effect, the resistive ballooning modes in the second stability regime may be nearly stabilized with compression. If the ion diamagnetic drift effect were also included, even stronger reduction of the growth rate is expected, similar to that found by Diamond *et al.*[7] in the first stability regime.

C. Effect of Parallel Thermal Conduction

Finally, we study the stabilizing effects associated with the temperature evolution, particularly, the parallel thermal conduction. Since the effect of compression was investigated in Sec. III.A, here we limit our interest to the incompressible case for which Eq. (7) reduces to $p = \phi + t$. Then, we obtain the following reduced equations from Eqs. (5)–(8):

$$\frac{\partial}{\partial\theta}\left[\left(1+\frac{i\widehat{\omega}_*}{\widehat{\gamma}}\right)\phi + \alpha_2\frac{i\widehat{\omega}_*}{\widehat{\gamma}}t\right] = \left[1+\frac{i\widehat{\omega}_*}{\widehat{\gamma}}(1+\alpha_2\eta_e)+\frac{\epsilon}{\widehat{\gamma}}f\right]\psi\ , \tag{19}$$

$$\frac{\partial}{\partial\theta}(f\psi) = \epsilon\widehat{\gamma}^2 f\phi - \frac{C}{1+\eta_e}(\phi+t)\ , \tag{20}$$

$$\alpha_3\nu\frac{\partial}{\partial\theta}\left[\frac{\partial t}{\partial\theta} - \left(\eta_e + \frac{i\alpha_1\epsilon}{\omega_*\alpha_3}f\right)\psi\right] = \alpha_4\epsilon^2 ft + \frac{3}{2}G\widehat{\gamma}(t-\eta_e\phi) + 5i\widehat{\omega}_*\epsilon_n G\frac{C}{\alpha}t\ . \tag{21}$$

As before, using the two length scale assumption we can derive an approximate analytic dispersion relation from Eqs. (19)–(21) as follows:

$$\left[\alpha_3\nu + \frac{3}{2}G\widehat{\gamma}(1+\eta_e)\right]\left[\frac{\alpha^2}{2} - (1+\eta_e)\widehat{\gamma}^3\left(1+\frac{i\widehat{\omega}_*}{\widehat{\gamma}}\right)\right]$$

$$= -\hat{\gamma}\left(1 - \alpha_1 \frac{i\hat{\omega}_*}{\hat{\gamma}}\right)\left[\frac{3}{2}\eta_e G\hat{\gamma}^3(1+\eta_e) - \frac{\alpha^2}{2}\left(\frac{\alpha_1\nu}{i\hat{\omega}_*} - \frac{5i\hat{\omega}_*\epsilon_n\eta_e G}{\alpha\epsilon}\right)\right] . \qquad (22)$$

First, we investigate the effect of parallel thermal conduction by varying the parameter ν. Figure 6 shows the growth rate and the real frequency as functions of ν obtained analytically and numerically. The analytical and numerical results, which agree quite well, both indicate that the parallel thermal conduction gives an insignificant effect on the stability. This feature is rather surprising and is in contrast with the case of the resistive ballooning modes driven by Δ', for which this term contributes to significant stabilization.[10]

In Sec. III.A, we found that the perpendicular magnetic compression term in the continuity equation, Eq. (7), gives a strong stabilizing effect. We note that a similar magnetic compression term also exists in the temperature evolution equation, i.e, the last term in Eq. (21). Therefore, it is of interest to investigate its effect, and the result is shown in Fig. 7. The result shows that the compression term has a negligible effect here, unlike the case with the continuity equation. This rather surprising feature seems to be caused by the existence of the factor i in the coefficient of the magnetic compression term in the temperature equation, which changes the phase of this term by $\frac{\pi}{2}$ so that it contributes differently.

In summary, we have found that the parallel thermal conduction and the magnetic compression term in the temperature evolution equation have insignificant effects on the non-Δ'-driven resistive ballooning modes with $\gamma \geq \gamma_s$.

IV. Conclusion

In the second stability regime, it is known that the resistive ballooning modes driven by Δ' in the ideal region are stabilized. However, there also exists another kind of resistive ballooning modes which can be unstable due to a different, non-Δ' driving force coming from the resistive region in the incompressible limit. In this paper, we have investigated the effect on these unstable modes in the second stability regime of various transport-type

terms such as compression, diamagnetic drift, and parallel thermal conduction, using the $s - \alpha$ tokamak equilibrium model. We find that the compression entering through the continuity equation gives a significant stabilizing effect, mainly through the perpendicular magnetic compression. This strong stabilization suggests the possibility of a second stable window where both kinds of resistive ballooning modes are stable. Diamagnetic drift effects slightly reduce the growth rate in the incompressible limit, but with compression they lead to fairly strong stabilization. The ion polarization compression, which becomes significant at large values of diamagnetic drift frequency, contributes to stabilization, unlike the case for the modes driven by Δ'. On the other hand, the parallel thermal conduction and the perpendicular magnetic compression in the temperature evolution equation are shown to have a negligible effect on the stability on the non-Δ' resistive ballooning modes, which is also different from the results for the case of the modes driven by Δ'.

References

1. A. Sykes, C.M. Bishop, and R.J. Hastie, Plasma Phys. Controlled Fusion **29**, 719 (1987).

2. G.Y. Fu, J.W. Van Dam, D.L. Holland, B.D. Fried, and A. Baños, Jr., UCLA Report No. PPG-1302 (April, 1990), to be published in Phys. Fluids.

3. A.B. Mikhailovskii and E.I. Yurchenko, Sov. J. Plasma Phys. **9**, 409 (1983).

4. J.Y. Kim and D.-I. Choi, Phys. Fluids B **1**, 1444 (1989).

5. T.C. Hender, K. Grassie, and H.P. Zehrfeld, Nucl. Fusion **29**, 1459 (1989).

6. T.C. Hender, B.A. Carreras, W.A. Cooper, J.A. Holmes, P.H. Diamond, and P.L. Similon, Phys. Fluids **27**, 1439 (1984).

7. P.H. Diamond, P.L. Similon, T.C. Hender, and B.A. Carreras, Phys. Fluids **28**, 1116 (1985).

8. J.Y. Kim, G.S. Cho, and D.-I. Choi, Phys. Fluids **31**, 2659 (1988).

9. A.K. Sundaram, A. Sen, and P.K. Kaw, Phys. Rev. Lett. **52**, 1617 (1984).

10. J.Y. Kim and D.-I. Choi, Phys. Fluids B **1**, 1026 (1989).

11. J.W. Connor and R.J. Hastie, Plasma Phys. **27**, 621 (1985).

12. M.E. Lord, M.R. Scott, and H.A. Watts, *Applied Nonlinear Analysis* (Academic Press, New York, 1979), p. 635.

Figure Captions

1. Growth rate $\hat{\gamma}$ as a function of the pressure gradient α for an incompressible plasma and a compressible plasma with $s = 1$, $\epsilon = 0.1$, $\beta = 0.1$, $M_\perp = 1$, and $\epsilon_n = 0.1$; also shown is the analytical estimate for the compressible case (dashed curve).

2. Growth rate $\hat{\gamma}$ versus the inverse aspect ratio ϵ_n for $\beta = 0$ and $\beta = 0.1$ with $\alpha = 4$, $s = 1$, $\epsilon = 0.1$, and $M_\perp = 1$.

3. Growth rate $\hat{\gamma}$ and real frequency $\hat{\omega}$ as functions of the diamagnetic drift frequency $\hat{\omega}_*$ in the incompressible case with $\alpha = 4$, $s = 1$, and $\epsilon = 0.1$.

4. Growth rate $\hat{\gamma}$ and real frequency $\hat{\omega}$ as functions of the diamagnetic drift frequency $\hat{\omega}_*$ in the compressible case with $\alpha = 4$, $s = 1$, $\epsilon = 0.1$, $\beta = 0.1$, $M_\perp = 1$, and $\epsilon_n = 0.1$.

5. Growth rate $\hat{\gamma}$ and real frequency $\hat{\omega}$ versus K_o in the compressible case with $\alpha = 4$, $s = 1$, $\epsilon = 0.1$, $\beta = 0.1$, $M_\perp = 1$, $\hat{\omega}_* = 1$, and $\epsilon_n = 0.1$, where K_o is a measure of the ion polarization compression.

6. Growth rate $\hat{\gamma}$ and real frequency $\hat{\omega}$ as functions of ν, where ν is a measure of the parallel thermal conductivity, with $\alpha = 4$, $s = 1$, $\epsilon = 0.1$, $\beta = 0.1$, $\hat{\omega}_* = 1$, $\eta_e = 1$, and $\epsilon_n = 0.1$: numerical results (solid curve) and analytical results (dashed curve).

7. Growth rate $\hat{\gamma}$ and real frequency $\hat{\omega}$ versus the inverse aspect ratio ϵ_n with $\alpha = 4$, $s = 1$, $\epsilon = 0.1$, $\beta = 0.1$, $\hat{\omega}_* = 1$, $\eta_e = 1$, and $\nu = 4$, when thermal conduction effects are included.

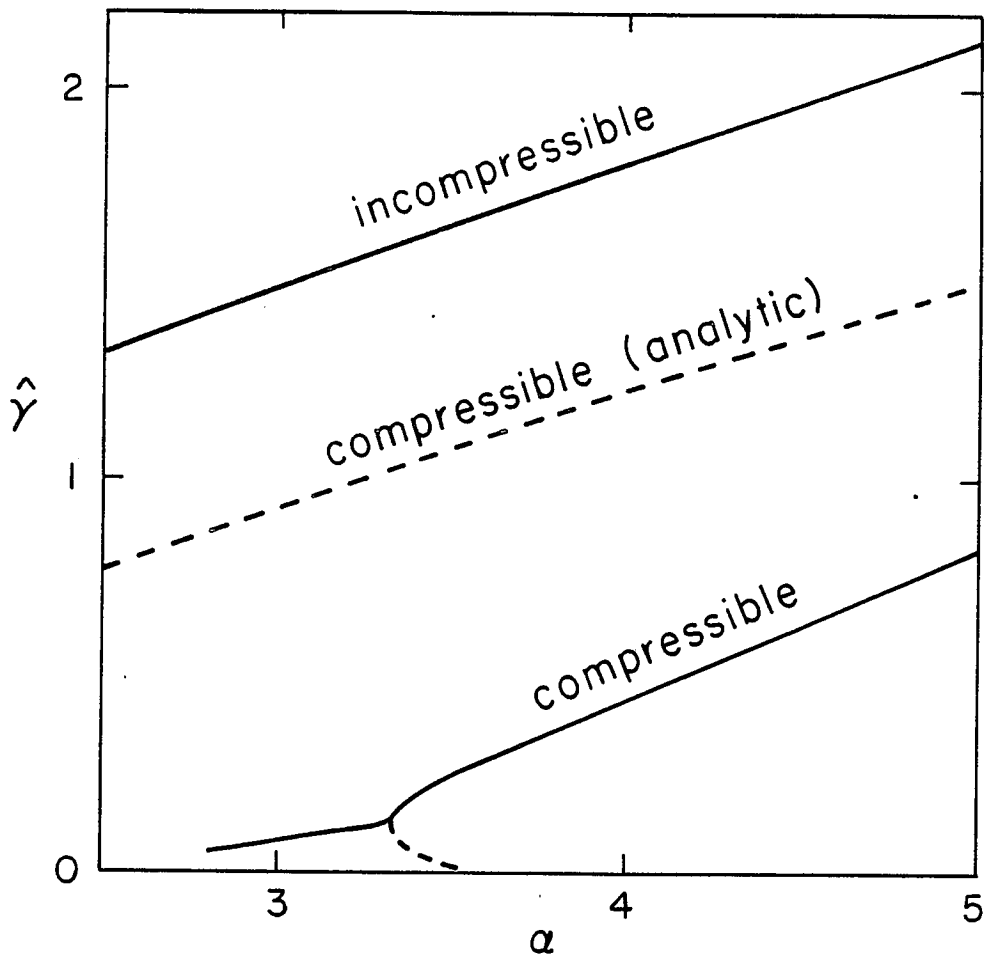
2
1
0
$\hat{\gamma}$
incompressible
compressible (analytic)
compressible
3
4
5
α

Fig. 1

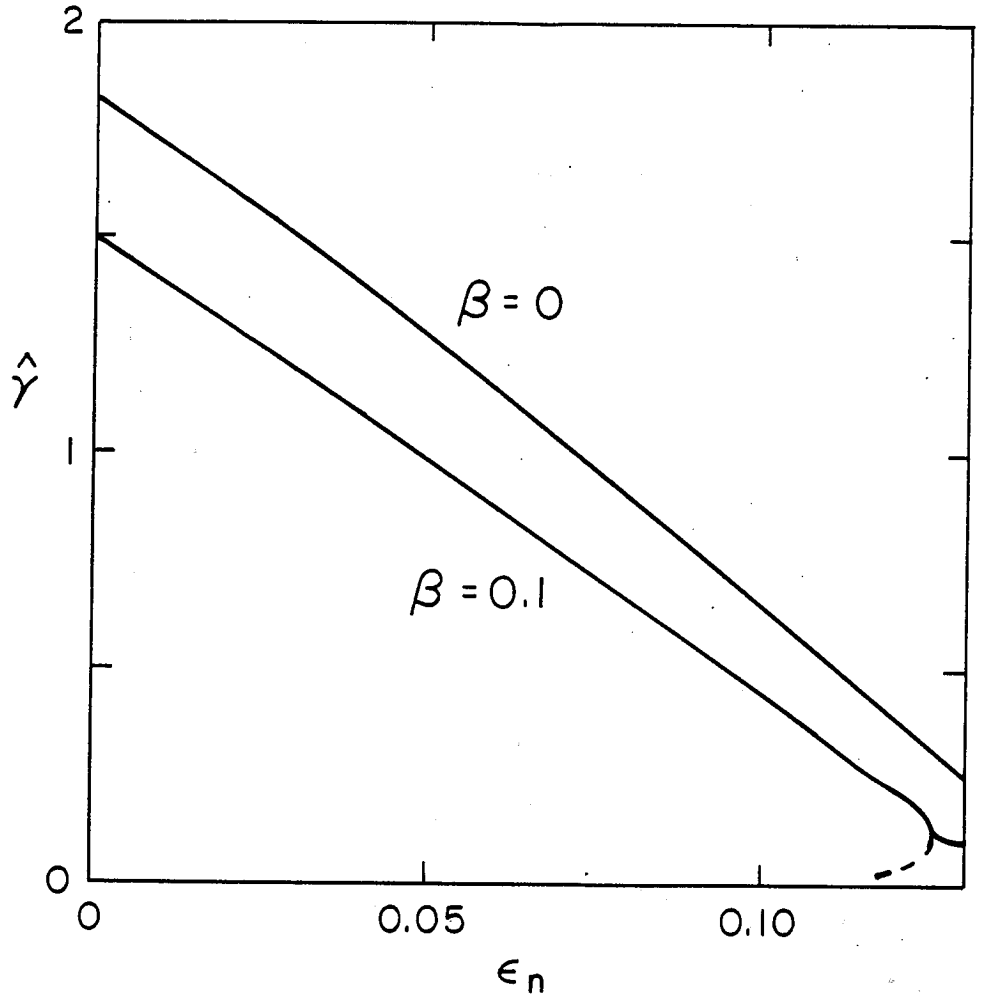

Fig. 2

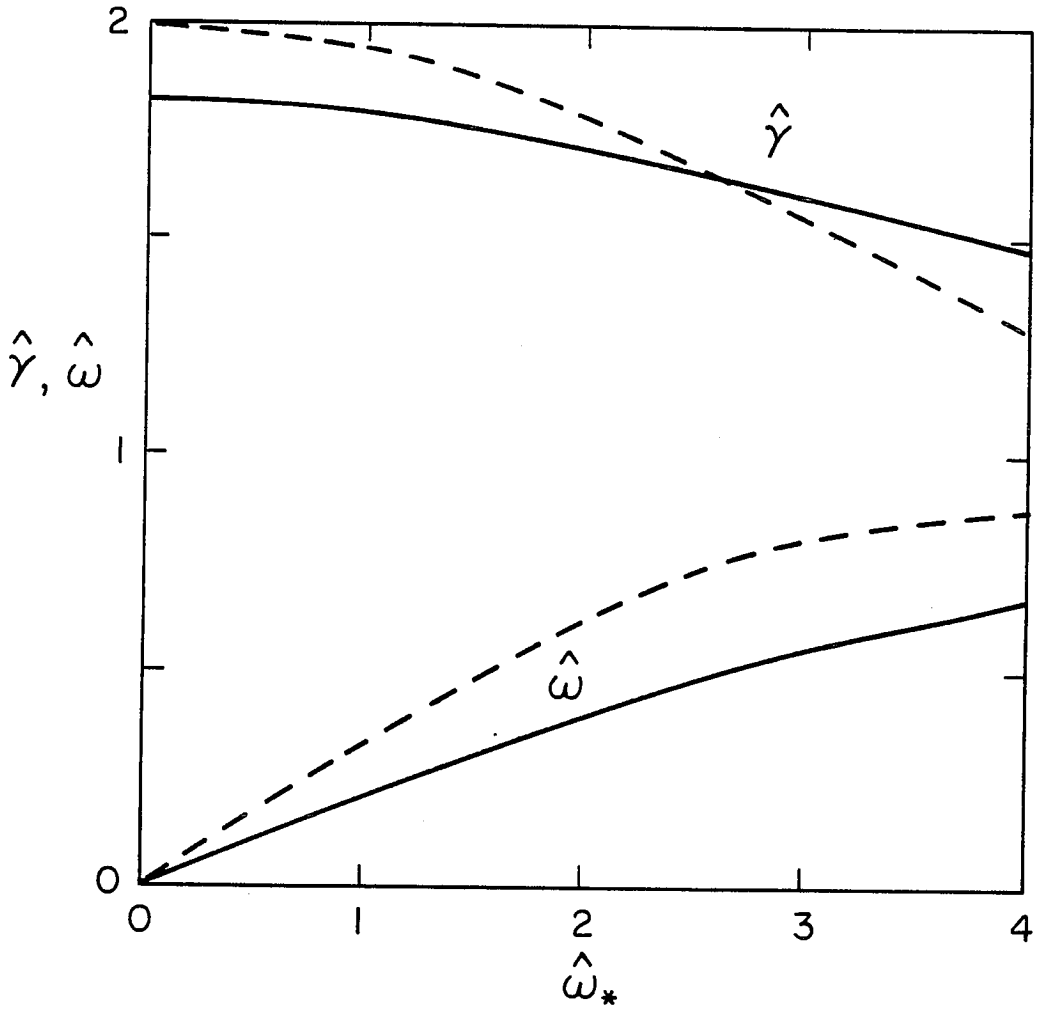

Fig. 3

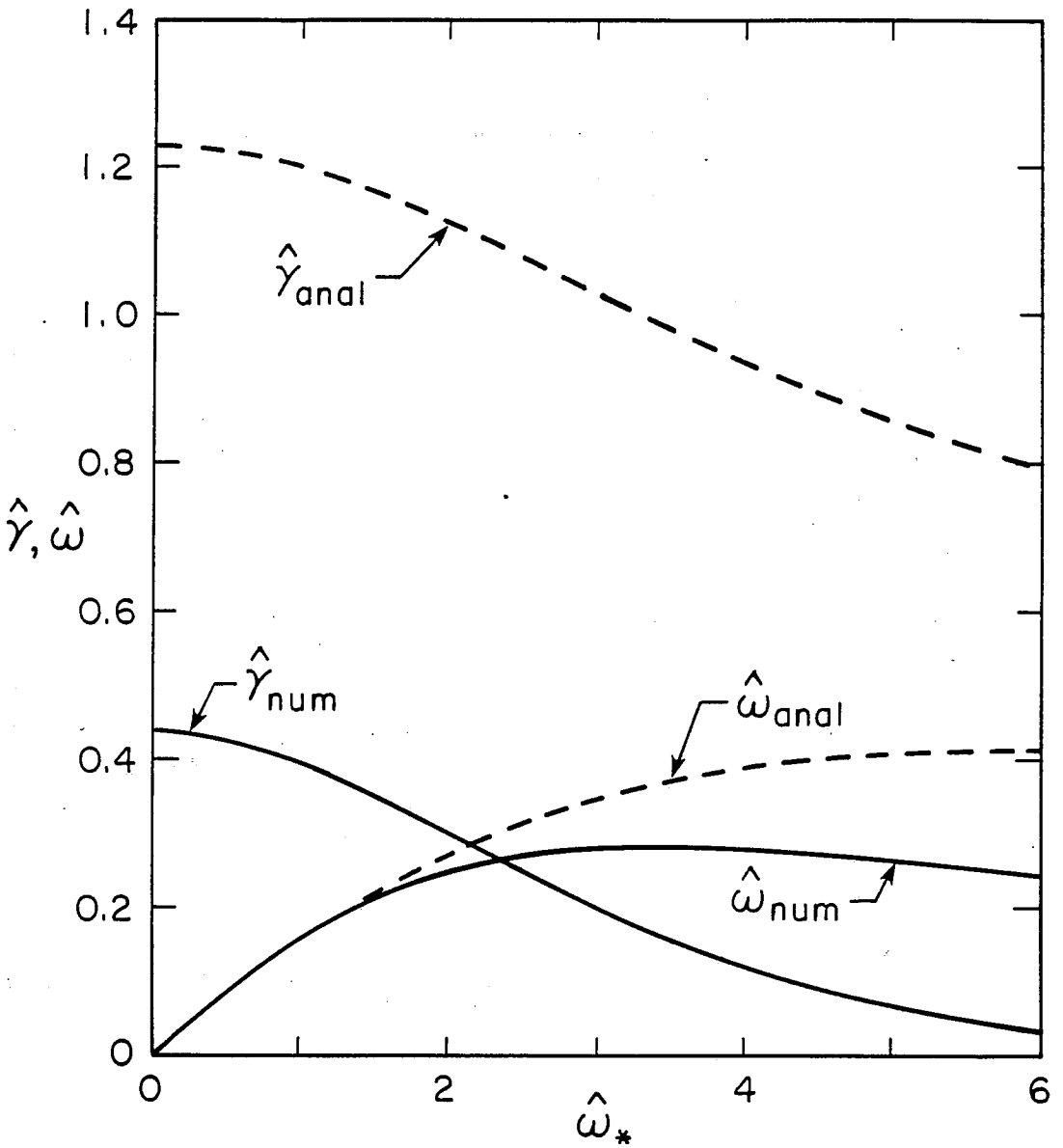
1.4
1.2
1.0
0.8
0.6
0.4
0.2
0
$\hat{\gamma}, \hat{\omega}$
$\hat{\gamma}_{anal}$
$\hat{\gamma}_{num}$
$\hat{\omega}_{anal}$
$\hat{\omega}_{num}$
0
2
4
6
$\hat{\omega}_*$

Fig. 4

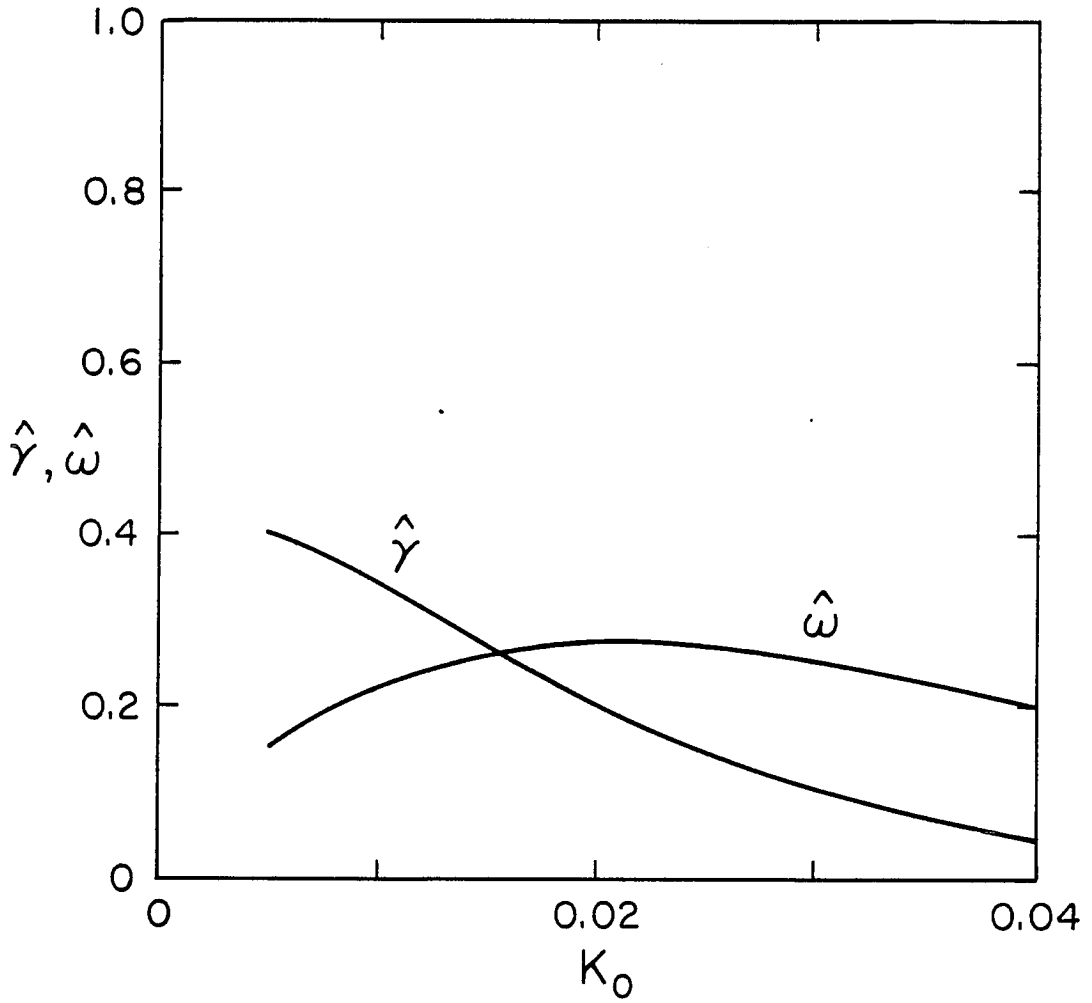
1.0
0.8
0.6
$\hat{\gamma}, \hat{\omega}$
0.4
0.2
0
$\hat{\gamma}$
$\hat{\omega}$
0
0.02
0.04
K_0

Fig. 5

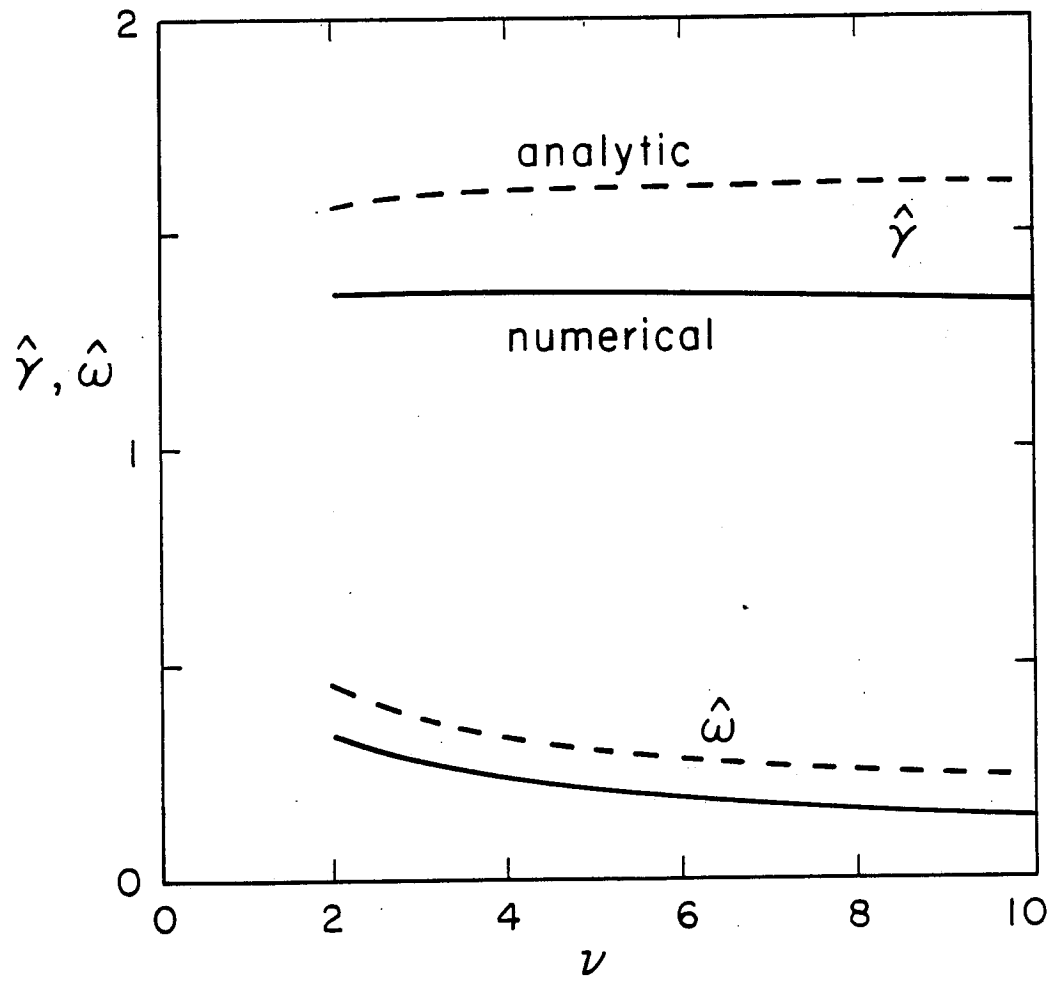
2
1
0
0
2
4
6
8
10
analytic
$\hat{\gamma}$
numerical
$\hat{\gamma}, \hat{\omega}$
$\hat{\omega}$
ν

Fig. 6

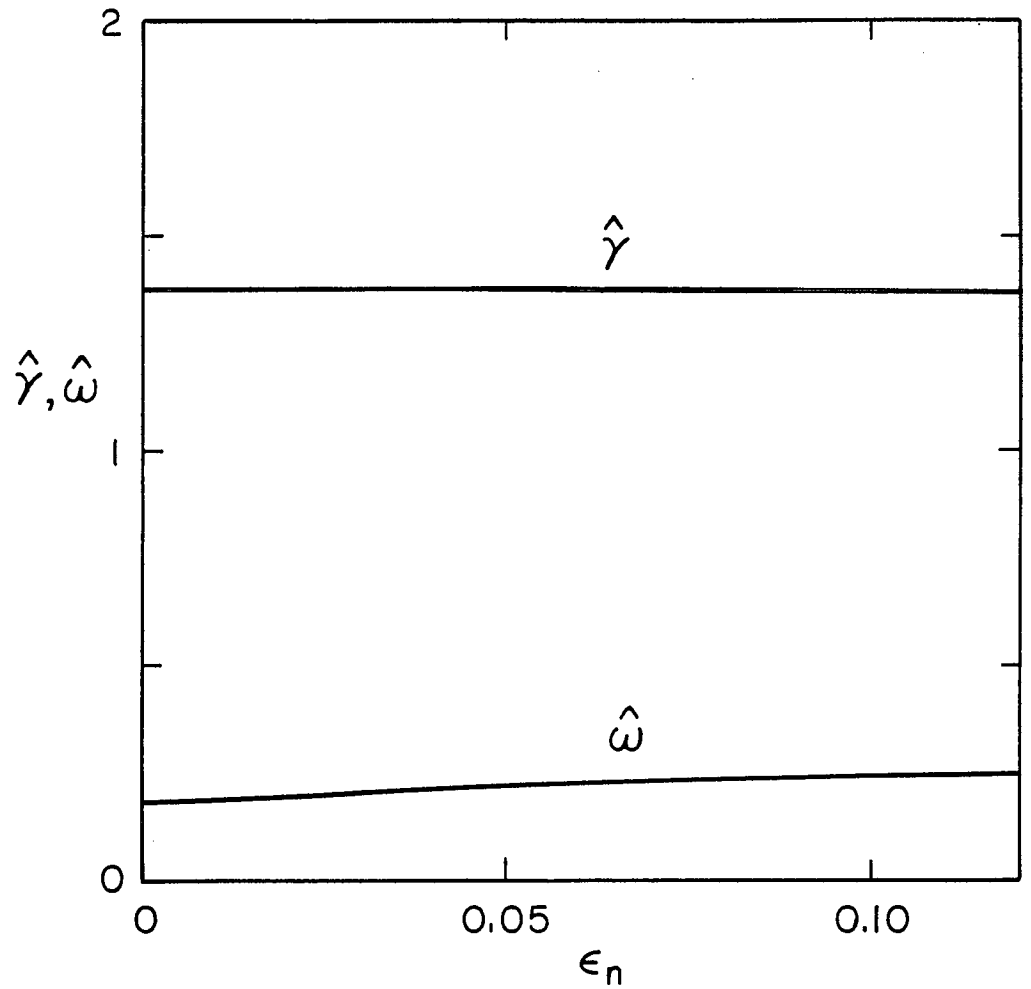
2
1
0
$\hat{\gamma}$
$\hat{\omega}$
$\hat{\gamma}, \hat{\omega}$
0
0.05
0.10
ϵ_n

Fig. 7